



A low-velocity conduit throughout the mantle in the robust component of a tomography model

N. Takeuchi¹

Received 3 February 2009; revised 13 March 2009; accepted 20 March 2009; published 15 April 2009.

[1] Detecting the roots of mantle plumes and constraining their connections to the Large Low Shear Velocity Provinces (LLSVPs) in the CMB region are critical problems for understanding mantle dynamics. Among the low-velocity conduits observed in the previous tomography models, the conduit beneath the Samoa/Tahiti region appears to be the most reliable because many models suggest it has a deep root. However, it is not clear whether the models are sufficiently accurate to confirm the reliability of this feature. In this study, we apply the singular value decomposition to confirm that this feature is well constrained by the data. The results indicate the plume beneath the Samoa/Tahiti region rising from the upper surface of the Pacific LLSVP. It might be a plume rising from a chemically distinct dome in the thermo-chemical convection. **Citation:** Takeuchi, N. (2009), A low-velocity conduit throughout the mantle in the robust component of a tomography model, *Geophys. Res. Lett.*, *36*, L07306, doi:10.1029/2009GL037590.

1. Introduction

[2] The depth from which plumes rise is one of the most critical problems for understanding mantle dynamics. Depth ranges of low-velocity conduits in seismic tomography models are potentially useful for revealing the roots of plumes. However, the resolution and accuracy of tomography models are limited, and whether or not a wide variety of low-velocity conduits have deep roots remains controversial [e.g., *Montelli et al.*, 2006; *Li et al.*, 2008]. We thus decided to focus on the most reliable conduits in the models. The conduit beneath the Samoa/Tahiti region appears to be the most reliable because a large number of studies have documented its deep origin [e.g., *Mégnin and Romanowicz*, 2000; *Zhao*, 2001; *Romanowicz and Gung*, 2002; *Montelli et al.*, 2004, 2006]. Some of these studies showed the significance of the focused feature by formal resolution tests. However, it is not clear whether the accuracy of these models is sufficient to confirm the plausibility of this feature.

[3] In this paper, I apply singular value decomposition [e.g., *Lanczos*, 1961] to confirm the accuracy of the conduit observed in model SH18CE [Takeuchi, 2007]. The results indicate that the conduit beneath the Samoa/Tahiti region is robust and is connected to the upper surface of the Pacific

LLSVP. The geophysical implications for these results are also presented.

2. Low-Velocity Conduit in Tomography Models

[4] Figure 1 shows the whole mantle SH velocity model, SH18CE [Takeuchi, 2007], which was obtained by waveform inversion based on three-dimensional Born kernels. The inversion fully utilized later phase information. The data set used includes body waveforms of major and multi-orbit phases, which were hardly used in previous studies. Such later phases significantly improve the data sampling in the upwelling regions [see *Takeuchi*, 2007, Figure 2], which improves resolution for plume images. Along the black lines in Figure 1, we can confirm a low-velocity conduit rising from the Pacific LLSVP. The conduit is a bit tilted in the north-south direction in the lower mantle and in the east-west direction in the upper mantle. The conduit appears to penetrate the 670 discontinuity and reach to the lithosphere (70 km depth). The continuity of this conduit is directly confirmed by the cross section (Figure 2b, left). To show the continuity, a section in the north-south direction for the lower mantle and a section in the east-west direction for the upper mantle are merged with each other.

[5] Such a conduit is not a unique feature to model SH18CE but has been confirmed in several other models. For example, the *S* velocity model shown in section A of *Mégnin and Romanowicz* [2000, Figure 11a], the *P* velocity model shown in section A of *Zhao* [2001, Figure 7], the *Q* model shown in the lower sections of *Romanowicz and Gung* [2002, Figure 3A], and the *P* and *S* velocity models shown by *Montelli et al.* [2006, Figures 21–22] show a similar feature. The data set and inversion techniques are independent among these studies, which indicates the robustness of the focused feature. To augment the evidence for this robustness, I will present the results obtained by a completely independent approach.

3. Method to Assess the Robustness

[6] Almost all tomography models inevitably include unreliable features that are not well constrained by the data (and are thus keenly sensitive to data errors). To assess the robustness of the observed features, the singular value decomposition (SVD) [e.g., *Lanczos*, 1961] is one of the most popular methods. Here we apply the SVD to solve a general linear inverse problem by using the method of *Wiggins* [1972]. We obtain solutions with various cutoff levels (i.e., various numbers of eigenvectors used to represent the solutions). We assess the robustness of the observed features by seeing whether or not the features exist in solutions with fewer eigenvectors. For rigorous assessment,

¹Earthquake Research Institute, University of Tokyo, Tokyo, Japan.

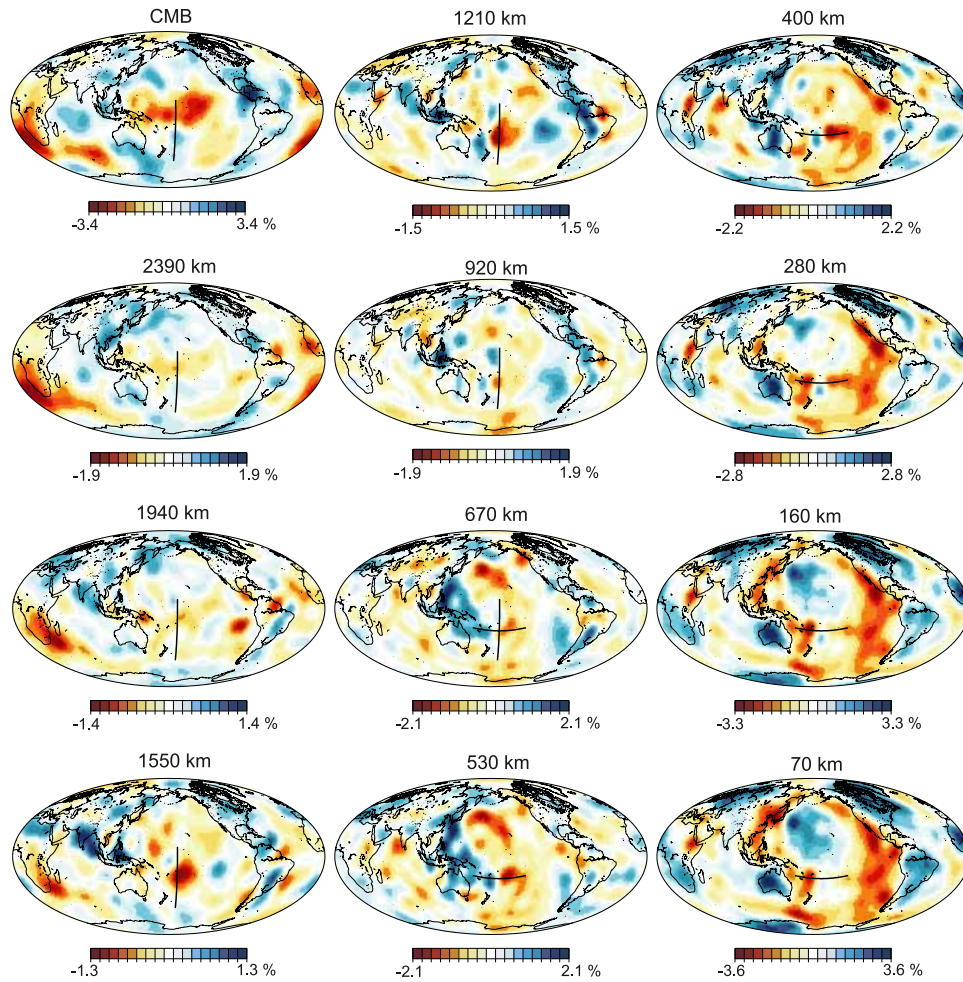


Figure 1. The low-velocity conduit observed in SH18CE [Takeuchi, 2007]. The conduit appears on the black lines in the figures. The color scales are normalized by the maximum absolute amplitude of lateral heterogeneity at each depth.

we might have to analyze the covariance and resolution matrices by taking both diagonal and off-diagonal elements into account [e.g., Oldenborger and Routh, 2009]. However, following the approach by Wiggins [1972], we here assume that the feature is robust if it is observed in the models with little degradation by data errors.

[7] We use the same data set, model parameters, and kernels as those used to obtain model SH18CE [Takeuchi, 2007]. For simplicity, we assume a linear dependency between the data and model parameters. For the case of typical tomography problems, the residuals between the observed data and the synthetic for the standard spherically symmetric model, $\delta\mathbf{d}$, are assumed to be well described by a linear equation for the model perturbation with respect to the standard model, $\delta\mathbf{m}$:

$$\delta\mathbf{d} = \mathbf{G} \delta\mathbf{m}, \quad (1)$$

where \mathbf{G} is a matrix to describe the linear dependency. Note that model SH18CE [Takeuchi, 2007] was obtained by using equation (1), and that many features observed in this model are consistent with those obtained by previous studies (using different types of data sets and inversion techniques).

The linearity assumption can thus be considered plausible at least for applications to model SH18CE.

[8] In the conventional SVD, we first solve the following eigenvalue problem:

$$\begin{pmatrix} \mathbf{0} & \mathbf{G} \\ \mathbf{G}^T & \mathbf{0} \end{pmatrix} \begin{pmatrix} \mathbf{u}_i \\ \mathbf{v}_i \end{pmatrix} = \lambda_i \begin{pmatrix} \mathbf{u}_i \\ \mathbf{v}_i \end{pmatrix}, \quad (2)$$

where λ_i is the i -th eigenvalue and \mathbf{u}_i and \mathbf{v}_i are the corresponding eigenvectors. We assume $\lambda_1 \geq \lambda_2 \geq \lambda_3 \geq \dots$ and that \mathbf{u}_i and \mathbf{v}_i are normalized so that their norm is equal to unity. In waveform tomography, the row number of matrix \mathbf{G} (i.e., the number of data) is usually huge. The dimension of matrix \mathbf{G} in our problem is $117,527,450 \times 5,054$, and it is not practical to directly solve equation (2). Furthermore, because we compute rigorous three-dimensional kernels [Takeuchi, 2007], \mathbf{G} is a full matrix. An approximated solution (e.g., Lanczos algorithm) is thus not very useful, as the methods utilize the sparseness of the matrix.

[9] However, we here want to obtain the appropriate solution for equation (1) rather than explicit eigenvalues and eigenvectors in equation (2). We can solve the inverse problem for equation (1) if we fully utilize the fact that matrix $\mathbf{G}^T \mathbf{G}$ ($5,054 \times 5,054$) can be directly decomposed in

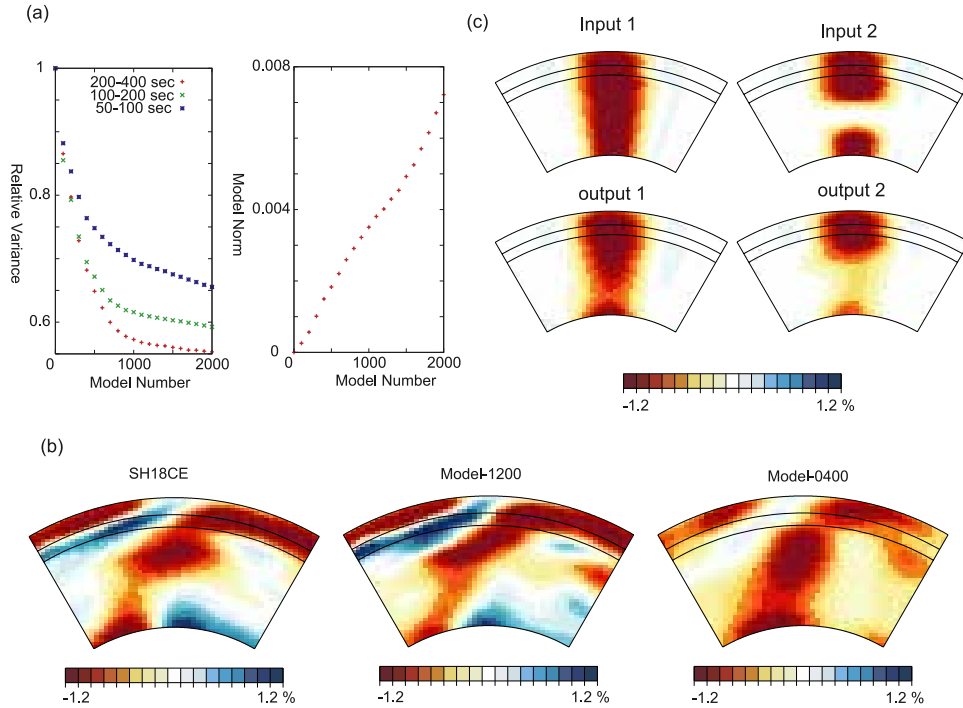


Figure 2. (a) The (left) relative variance and (right) model norm as a function of the model number (see the text for definitions). Red, green, and blue symbols in Figure 2a (left) denote variance for the waveform data for three different periodic bands (200–400 sec, 100–200 sec, and 50–100 sec, respectively). (b) Comparison of cross sections for the black lines shown in Figures 1, 3, and 4. Model SH18CE [Takeuchi, 2007] and the models obtained in the present study (Model-1200 and Model-0400) are compared. The north-south section for the lower mantle and the east-west section for the upper mantle are merged with each other. The color scale is saturated if the anomalies are greater than 1.2% or less than -1.2% . (c) The results of the resolution tests for Model-1200. (top) Input models have low-velocity conduits with -1.5% velocity anomalies. (bottom) We recovered each input model following the inversion scheme used to obtain Model-1200 and obtained the output models shown. The sections at the same locations are shown by using the same color as those in Figure 2b.

a practical CPU time. We first solve the following eigenvalue problem to obtain all of eigenvalues λ_i and eigenvectors \mathbf{v}_i :

$$(\mathbf{G}^T \mathbf{G}) \mathbf{v}_i = \lambda_i^2 \mathbf{v}_i. \quad (3)$$

Note that, in our problem, all eigenvalues are non-zero and different from each other. We then compute the solution with P eigenvectors, $\delta \hat{\mathbf{m}}_P$, as follows:

$$\delta \hat{\mathbf{m}}_P = \sum_{i=1}^P \mathbf{v}_i^T \{ (\mathbf{G}^T \mathbf{G})^{-1} \mathbf{G}^T \delta \mathbf{d} \}. \quad (4)$$

Note that $\{ (\mathbf{G}^T \mathbf{G})^{-1} \mathbf{G}^T \delta \mathbf{d} \}$ is the ordinary least-squares solution. Note also that the i -th component of $\delta \hat{\mathbf{m}}_P$ is the projection of the ordinary least-squares solution to the i -th basis vector (or eigenvector). From equations (3) and (4), we see that this algorithm does not require decomposition of the huge matrix in l.h.s. of equation (2) but requires only the decomposition of $(\mathbf{G}^T \mathbf{G})$.

4. Robust Features in the Model

[10] We now extract the robust features by comparing the solutions with various cutoff levels. We assigned model numbers according to the number of eigenvectors used to obtain the model (i.e., the model number is equal to P).

The 0-th model denotes the initial spherically symmetric model (i.e., $\delta \hat{\mathbf{m}}_0 = \mathbf{0}$). The variance of the residuals between the data and the synthetic for each model, $|\delta \mathbf{d} - \mathbf{G} \delta \hat{\mathbf{m}}_P|^2 / |\delta \mathbf{d}|^2$, is compared (Figure 2a, left). Note that the variance is normalized by that for the initial model, $|\delta \mathbf{d}|^2$. The norm of each model, $|\delta \hat{\mathbf{m}}_P|^2$, is also compared (Figure 2a, right).

[11] Our data set consists of waveforms with three different periodic bands (200–400 sec, 100–200 sec, 50–100 sec) [Takeuchi, 2007]. For the longer period data set (200–400 sec), the variance rapidly decreases for the first 800 models and becomes almost invariant for the latter models. For the shorter period data set (50–100 sec), the variance rapidly decreases for the first 400 models and continues to moderately decrease until the 2000-th model. The norm of the models, more or less, linearly increases as the model number increases (Figure 2a, right), but the increase in the norm is relatively gentle between the 800-th and 1200-th models.

[12] Because the variance continues to reasonably improve as the model norm increases gently, $P = 1200$ should be one of reasonable cutoff levels. We therefore assume the 1200-th model (hereafter called Model-1200; shown in Figure 3) as the optimal model. Because the variance for every periodic band continues to rapidly improve for the first 400 models, we assume that the 400-th model (hereafter called Model-0400; shown in Figure 4) is the robust component of the optimal model.

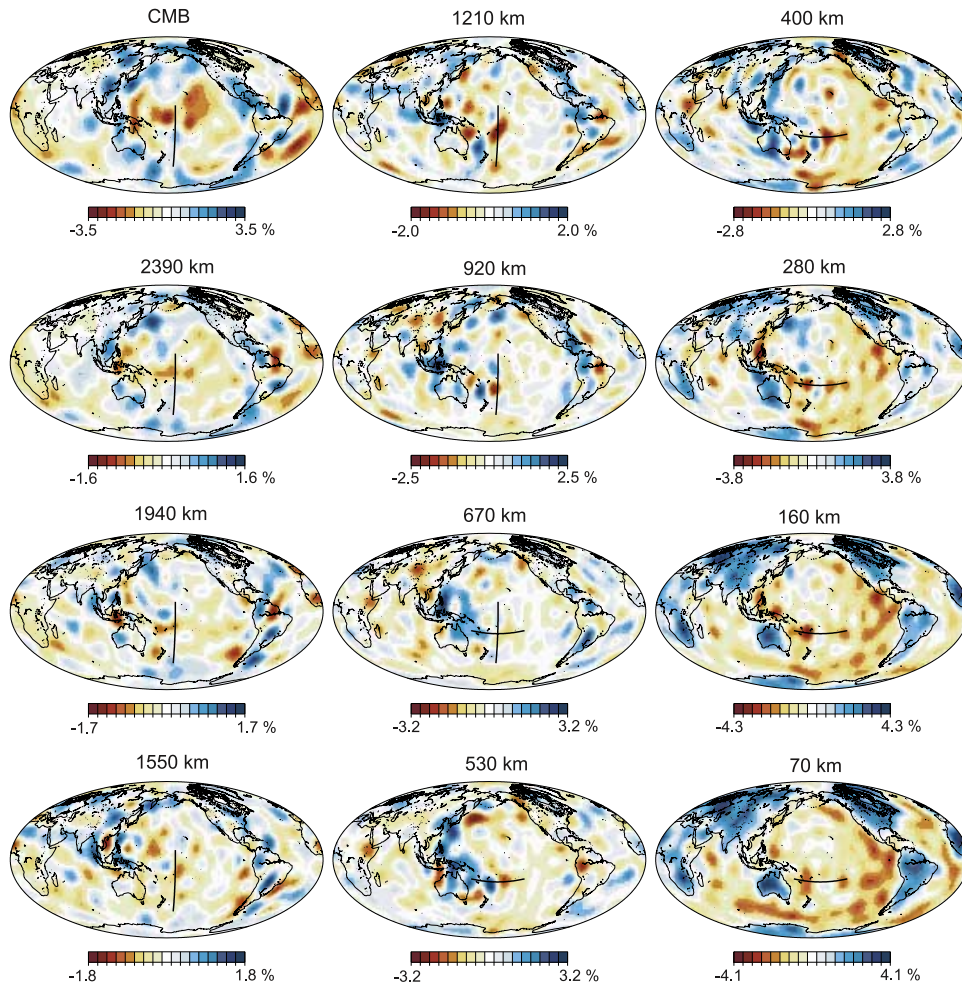


Figure 3. The same as Figure 1 except that Model-1200 is shown.

[13] Model-1200 is generally consistent with model SH18CE [Takeuchi, 2007] and other previous models. We compute the correlation coefficients between SH18CE and Model-1200 for the 12 depths shown in Figures 1 and 3. The correlation coefficient is 0.72 on average, the highest is 0.85 (160 km depth), and the lowest is 0.59 (1940 km depth). The results suggest that Model-1200 can be assumed to be one of the reasonable models that retrieve many of the consistent features commonly observed in recent tomography models. Comparing the cross section for the conduit beneath the Samoa/Tahiti region between SH18CE and Model-1200 (Figure 2b), we observe a similarity, which confirms that the choice of the cutoff level was reasonable.

[14] In contrast, Model-0400 is less consistent with both Model-1200 and SH18CE. The average correlation coefficients to Model-1200 and SH18CE are only 0.41 and 0.42, respectively. Nonetheless, Model-0400 has a reasonable variance reductions: it is 76% of that achieved by Model-1200. These results suggest that Model-0400 shows a robust component of Model-1200. Regardless of the poor correlation in global heterogeneity patterns, we can observe similarity in the cross sections for the conduit beneath the Samoa/Tahiti region (Figure 2b). This result indicates that this feature is one of the most robust features.

[15] Because every tomography model has limited resolution, we cannot rule out possibilities to have small-scale

discontinuities in the conduit. However, we conducted resolution tests for Model-1200 and confirmed that large-scale discontinuities (more than 500 km long) are unlikely to exist (Figure 2c). We recovered the input model with a discontinuous conduit by using the inversion scheme used to obtain Model-1200. The discontinuity is located between about 1500–2000 km depths where we have relatively weak anomalies in Model-1200 (Figure 2b). The recovered model clearly shows a discontinuity in that depth range (Figure 2c; right). In contrast, if the input model has a conduit throughout the mantle, we can recover continuous anomalies (Figure 2c, left).

5. Discussion

[16] Comparing the nature of the Pacific and African LLSVPs, we can see the similarities and differences. The African LLSVP is known to have strong low-velocity anomalies extending for more than 1000 km from the CMB [e.g., Ritsema *et al.*, 1997; Ni *et al.*, 2002]. It is also known to have sharp sides [e.g., Ni *et al.*, 2002] and an anomalous $\delta V_s/\delta V_p$ ratio [e.g., Wang and Wen, 2007]. From these observations, the African LLSVP is considered a chemically distinct dome.

[17] Because the Pacific LLSVP is also suggested to have sharp sides [e.g., To *et al.*, 2005; Takeuchi, 2008] together

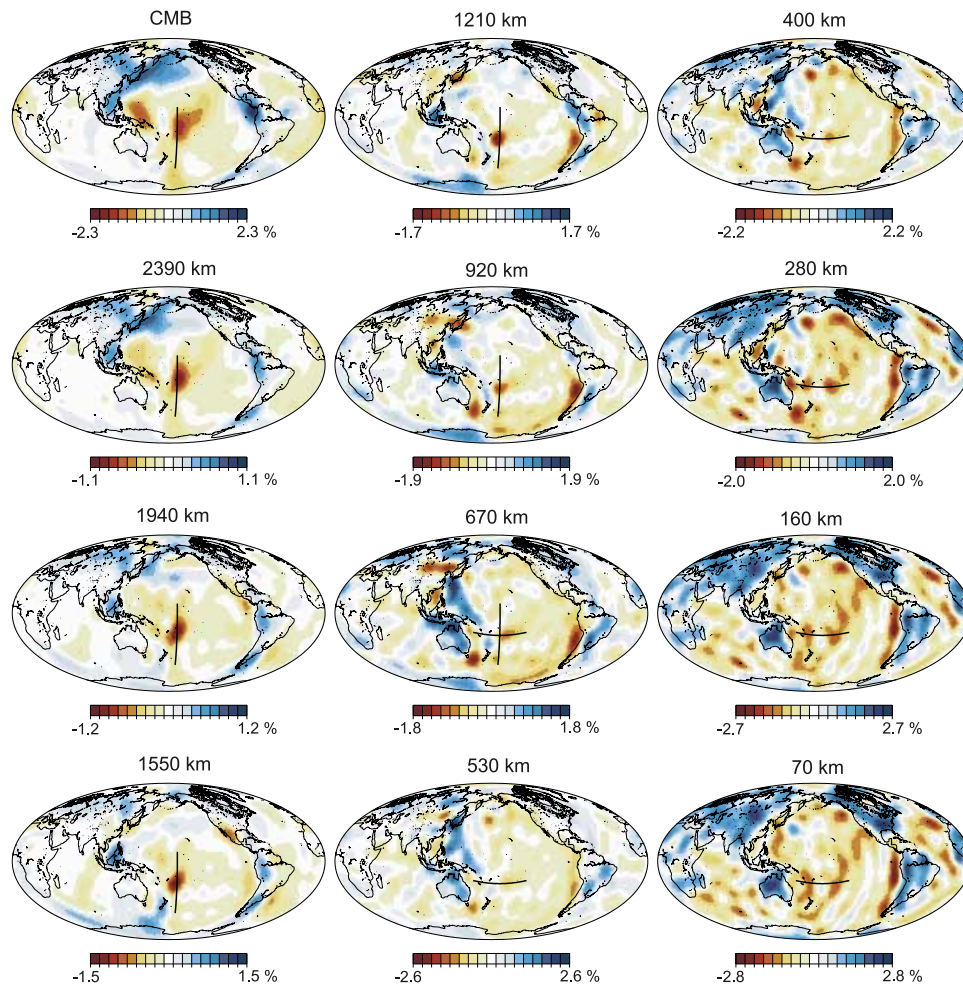


Figure 4. The same as Figure 1 except that Model-0400 is shown.

with an anomalous $\delta V_s/\delta V_p$ ratio [e.g., *Masters et al.*, 2000], it is probably also a chemically distinct dome. However, the vertical extent of the Pacific LLSVP is suggested to be far less than 1000 km [*Takeuchi*, 2007; *Takeuchi et al.*, 2008], which is definitely different from that for the African LLSVP.

[18] One scenario that explains these observations should be that the vertical extent of these two domes varied with time (e.g., the doming regime of convection suggested by *Davaille* [1999]). Similarities in features other than the vertical extent can be explained. *Davaille* [1999] predicted that the plumes rise from the upper surface of the chemically distinct domes. The low-velocity conduit beneath the Samoa/Tahiti region, which the present study showed to be a robust feature, can be interpreted as such a plume from the Pacific LLSVP.

[19] **Acknowledgments.** We are grateful for the use of the SGI ALTIX4700 at the Earthquake Research Institute, University of Tokyo; the HA8000 at the Information Technology Center, University of Tokyo; and the Earth Simulator at the Japan Agency for Marine-Earth Science and Technology. Comments by anonymous reviewers were very helpful.

References

Davaille, A. (1999), Simultaneous generation of hotspots and superswells by convection in a heterogeneous planetary mantle, *Nature*, *402*, 756–760.
Lanczos, C. (1961), *Linear Differential Operators*, 564 pp., D. Van Nostrand, London.

Li, C., R. D. van der Hilst, E. R. Engdahl, and S. Burdick (2008), A new global model for P wave speed variations in Earth's mantle, *Geochem. Geophys. Geosyst.*, *9*, Q05018, doi:10.1029/2007GC001806.
Masters, G., G. Laske, H. Bolton, and A. Dziewonski (2000), The relative behavior of shear velocity, bulk sound speed, and compressional velocity in the mantle: Implications for chemical and thermal structure, in *Earth's Deep Interior: Mineral Physics and Tomography From the Atomic to the Global Scale*, *Geophys. Monogr. Ser.*, vol. 117, edited by S. Karato et al., pp. 63–87, AGU, Washington, D. C.
Mégnin, C., and B. Romanowicz (2000), The three-dimensional shear velocity structure of the mantle from the inversion of body, surface and higher-mode waveforms, *Geophys. J. Int.*, *143*, 709–728.
Montelli, R., G. Nolet, G. Masters, F. A. Dahlen, and S.-H. Hung (2004), Global P and PP traveltime tomography: Rays versus waves, *Geophys. J. Int.*, *158*, 637–654.
Montelli, R., G. Nolet, F. A. Dahlen, and G. Masters (2006), A catalogue of deep mantle plumes: New results from finite-frequency tomography, *Geochem. Geophys. Geosyst.*, *7*, Q11007, doi:10.1029/2006GC001248.
Ni, S. D., E. Tan, M. Gurnis, and D. V. Helmberger (2002), Sharp sides to the African superplume, *Science*, *296*, 1850–1852.
Oldenborger, G. A., and P. S. Routh (2009), The point-spread function measure of resolution for the 3-D electrical resistivity experiment, *Geophys. J. Int.*, *176*, 405–414.
Ritsema, J., E. Garnero, and T. Lay (1997), A strong negative shear velocity gradient and lateral variability in the lowermost mantle beneath the Pacific, *J. Geophys. Res.*, *102*, 20,395–20,411.
Romanowicz, B., and Y. Gung (2002), Superplumes from the core-mantle boundary to the lithosphere: Implications for heat flux, *Science*, *296*, 513–516.
Takeuchi, N. (2007), Whole mantle SH velocity model constrained by waveform inversion based on three-dimensional Born kernels, *Geophys. J. Int.*, *169*, 1153–1163.

- Takeuchi, N., Y. Morita, N. D. Xuyen, and N. Q. Zung (2008), Extent of the low-velocity region in the lowermost mantle beneath the western Pacific detected by the Vietnamese broadband seismograph array, *Geophys. Res. Lett.*, *35*, L05307, doi:10.1029/2008GL033197.
- To, A., B. Romanowicz, Y. Capdeville, and N. Takeuchi (2005), 3D effects of sharp boundaries at the border of the Africa and Pacific superplumes: Observation and modeling, *Earth Planet. Sci. Lett.*, *233*, 137–153.
- Wang, Y., and L. X. Wen (2007), Geometry and P and S velocity structure of the “African Anomaly,” *J. Geophys. Res.*, *112*, B05313, doi:10.1029/2006JB004483.
- Wiggins, R. A. (1972), The general linear inverse problem: Implication of surface waves and free oscillations for Earth structure, *Rev. Geophys. Space Phys.*, *10*, 251–285.
- Zhao, D. (2001), Seismic structure and origin of hotspots and mantle plumes, *Earth Planet. Sci. Lett.*, *192*, 251–265.
-
- N. Takeuchi, Earthquake Research Institute, University of Tokyo, Tokyo 113-0032, Japan. (takeuchi@eri.u-tokyo.ac.jp)